Photoelectronic characterization of IgG antibody molecule–quantum dot hybrid as biosensing probe

2010 Nanotechnology 21 425501

(http://iopscience.iop.org/0957-4484/21/42/425501)

Nanotechnology **21** (2010) 425501 (11pp) doi:10.1088/0957-4484/21/42/425501

Photoelectronic characterization of IgG antibody molecule–quantum dot hybrid as biosensing probe

Hye-Weon Yu[1], Jinwook Lee[2], Sungyoun Kim[2], Sung-Jo Kim[1] and In S Kim[1,2,3]

[1] School of Environmental Science and Engineering, Gwangju Institute of Science and Technology (GIST), 261 Cheomdan-gwagiro, Buk-gu, Gwangju 500-712, Republic of Korea
[2] Center for Seawater Desalination Plant, Gwangju Institute of Science and Technology (GIST), 261 Cheomdan-gwagiro, Buk-gu, Gwangju 500-712, Republic of Korea

E-mail: iskim@gist.ac.kr

Received 4 August 2010
Published 22 September 2010
Online at stacks.iop.org/Nano/21/425501

Abstract
Quantum dot (QD)-based biomolecule hybrids have recently attracted much attention in specifically identifying and labeling target proteins. In this study, QD encapsulated with immunoglobulin antibodies, as a labeling building block in biosensors, was investigated to clarify the most efficient configuration and photoluminescence behavior. Both the biological recognition capacity and photoluminescence emitting signal of the antibody-coupled nanocrystal were validated through a photoelectrical characterization procedure. Derivation of the optimum number of antibody molecules to be packed onto the QD surface yielded the highest binding capacity for the target antigen. During formation of the bioactive layer, the intrinsic photoluminescence response of the QDs significantly decreased due to photoinduced hole transfer according to their rearranged electronic structure. The thorough study of this assembly provides a validation approach for the careful titration of biosensor probes for optimal reaction kinetics. Furthermore, it contributes to the development of an effective tool for the application and interpretation of QD-based labeling techniques.

(Some figures in this article are in colour only in the electronic version)

1. Introduction

Quantum dots (QDs), colloidal fluorescent semiconductor nanocrystals, have inherent advantages such as size-tunable photoluminescence, high quantum yield, high molar extinction coefficients, and high photostability [1–3]. Hence, QDs have recently attracted significant attention as a useful tool for the *in vitro* and *in vivo* imaging of proteins in cells [4–6], diagnostic immunoassays or biosensors [7–9], and in QD-based electronics such as light emitting diodes (LEDs) [10, 11] and photovoltaic cells [12] for a diverse range of biological, medical, environmental, and photoelectronic applications.

In particular, to hybridize the distinctive features of QDs for a biological system, in terms of labeling, sensing, and imaging, physicochemical modification of the QD surface using biomolecules such as immunoglobulin, peptides, or other proteins targeting a ligand of interest is required. For these optimized QD-based labeling techniques, characterization of QD encapsulated biomolecules by quantifying biomolecular elements linked to the nanocrystal is also needed. As such, an optimally designed supramolecular heterostructure would not only provide a more effective experimental procedure for manipulating the nanobiological system, but also assist in avoiding the pitfalls that could result in misinterpreting the biological data [13, 14].

Although the properties of individual components capable of revealing hybrid materials have been well documented over the years, characterization of the entire assembly has suffered from certain drawbacks and thus is still challenging. For example, transmission electron microscopy (TEM) is often useful for visualizing the shape and size

[3] Author to whom any correspondence should be addressed.

of an inorganic material, although it is not suitable for assessing the biomolecular coating on inorganic nanoparticles, due to the dryness of the active molecular element [13]. Electrophoresis has also been utilized to evaluate composites, but characterization is hindered by the strong charge of the nanocrystal [15] (appendix A). And even though bovine serum albumin (BSA) assays have been exploited to determine the concentration of proteins bound to nanocrystals [16], they are limited in their ability for use in the recovery of an analyzed sample.

In this work, our goal is to provide a framework for the photoelectric characterization of QDs encapsulated with immunoglobulin G (IgG) antibody (Ab) molecules for use as the building block of a labeling element in biosensor. The conjugate is examined in terms of the dual functional parts for the biological recognition layer, namely an IgG Ab molecule and the photoluminescence emitting center of a QD, as photoelectric characterization is suitable for assessing not only the biomolecular coating but also the nanocrystal. The configuration picture and photoluminescence behavior of the versatile heterogeneous hybrid were explored in three nanoscopic views: (1) investigation of the photoelectric behavior of discrete QDs and IgG Ab molecules, (2) verification of IgG Ab molecules docking on the QD surface, and (3) elucidation of the photoelectric response of QDs encapsulated with IgG Ab molecules. Herein, the biomolecular recognition elements tethered to one QD were quantified based on a stoichiometry-dependent modification for optimizing the binding capacity of the target antigen, which is essential for clarifying the configuration design of the labeling unit. The careful titration of the exact amount of IgG Ab molecules per QD is also important for optimal reaction kinetics. Furthermore, a precise interpretation of the photoluminescence emitting center in the QD can provide a fundamental understanding of the transfer pathway of the photogenerated-electrons and holes between QDs and the IgG Ab molecules.

2. Material and methods

2.1. Reagents

IgG Ab (MC10E7), against the cyanobacterial hepatotoxin microcystin-LR, as a model antigen, was obtained from Alexis, and QDs with a Qdot525 Antibody Conjugation Kit were purchased from Invitrogen.

2.2. Determination of the electronic structure of the discrete IgG Ab molecule and QD

To estimate the energetic band structure of the IgG Ab molecule-encapsulated QD, the highest occupied molecular orbital (HOMO), the lowest unoccupied molecular orbital (LUMO), and the band gap of each IgG Ab molecule and QD were determined using either optical or electrochemical measurements.

In the case of optical measurements, only band gap energies were obtained, using two spectroscopic methods: ultraviolet/visible (UV/vis) absorption spectra were recorded using a UV/vis spectrophotometer (Shimadzu), and the photoluminescence spectra and contour diagrams of the excitation–emission matrix (EEM) were plotted using an F-2500 fluorescence spectrophotometer (Hitachi).

In the electrochemical approach, the oxidation and reduction potentials of IgG Ab molecules and QDs were measured using cyclic voltammetry. These electrochemical experiments were carried out using an Autolab PGSTAT 302N potentiostat/galvanostat workstation (Eco Chemie) having a three-electrode system: a Au disk working electrode (0.8 mm radius), a Pt wire counter electrode, and a Ag/AgCl reference electrode. 0.1 M tetrabutylammonium hexafluorophosphate ($TBAPF_6$) in acetonitrile was used as the electrolyte for all electrochemical measurements. All cell potentials were referenced against a ferrocene/ferrocenium (FOC) redox couple as the internal standard. Since the 0.42 V half-wave potential ($E_{1/2}$) of FOC against Ag/AgCl corresponds to 4.8 eV below the vacuum level [17], the HOMO and LUMO levels were calculated, based on the oxidation and reduction peak potentials [18, 19], using

$$\text{HOMO (eV)} = -4.8 - (E^{\text{ox}}_{\text{peak}} - E_{1/2}\ \text{of FOC}). \quad (1)$$

2.3. Stoichiometry-dependent encapsulation of IgG Ab molecules on the QD surface

The IgG Ab molecules covalently conjugated to QDs, based on the following stoichiometry-based calculations (figure 1). (1) QDs were activated for 1 h using a heterobifunctional crosslinker, 4-(maleimidomethyl)-cyclohexanecarboxylic acid *N*-hydroxysuccinimide ester (SMCC), yielding a maleimide functionalized nanocrystal surface. (2) IgG Ab molecules were reduced for 30 min using dithiothreitol (DTT) to introduce free sulfhydryls. (3) Excess salts were removed separately from the QD or IgG Ab solutions via a NAP-5 column. (4) The reduced IgG Ab molecules (volume x) were coated onto the activated nanocrystal surface (volume y) over a 1.5 h period, with the following N_{Ab}:N_{QD} molar ratios.

$$N_{\text{Ab}} = \frac{1\ \mu\text{g Abs}}{\mu\text{l}} \times \frac{\text{Ab}}{2.475 \times 10^{-19}\ \text{g}} \times (x)\mu\text{l} \times \frac{g}{10^6\ \mu\text{g}} \quad (2)$$

$$N_{\text{QD}} = \frac{4\ \mu\text{mol QD}}{1} \times \frac{6.023 \times 10^{23}\ \text{QD particles}}{\text{mol}} \times (y)\ \mu\text{l} \times \frac{\text{mol}}{10^6\ \mu\text{mol}} \times \frac{1}{10^6\ \mu\text{l}}. \quad (3)$$

(5) The conjugation reaction was quenched for 30 min using β-mercaptoethanol, which reacts with any remaining maleimide functional groups on the QDs and converts them to non-reactive derivatives. (6) The IgG Ab molecule-conjugated QD suspension was then purified by multiple rounds of washing and centrifugation through an ultrafiltration membrane (100 kD cutoff) at 2000 rpm for 15 min to remove excess Ab cleaves and salts. (7) The final complex was resuspended and kept in 20 mM sodium tetraborate at 4 °C prior to use.

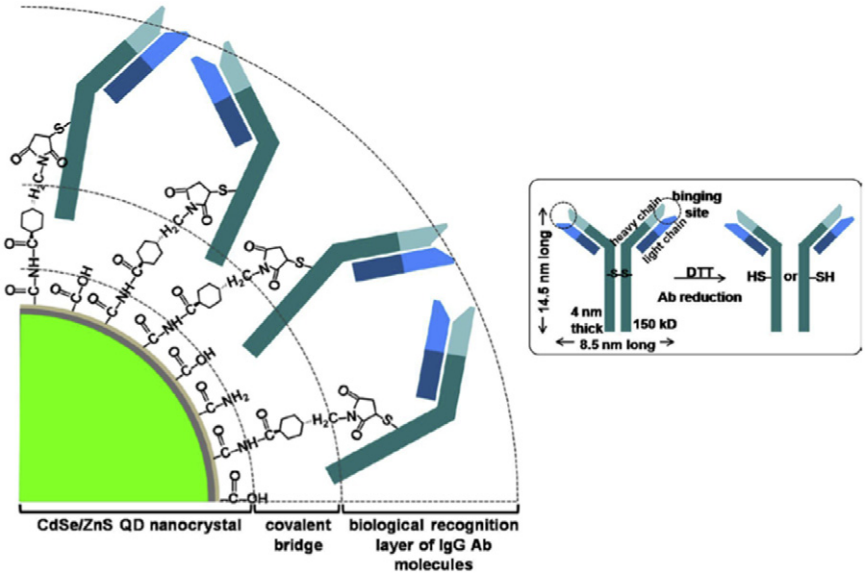

Figure 1. Conceptual configuration of CdSe/ZnS QD nanocrystals covalently coupled with functionalized IgG Ab molecules via a heterobifunctional crosslinker. The building block involves three components: QDs, an interfacial covalent linkage, and a biological recognition layer of IgG Ab molecules. The IgG Ab molecule is reduced using DTT to introduce free sulfhydryls, as shown in the inset [36, 37].

2.4. X-ray photoelectron spectroscopy (XPS) measurement of IgG Ab molecule-coated QD assembly

The surface compositions of the QDs, IgG Ab molecules, and the QD–IgG Ab molecule hybrid were analyzed to verify that the biomolecules covalently bound to the nanocrystal surface, using an XPS (Thermo VG Scientific, MultiLab 2000) with Avantage software. The base pressure in the XPS analysis chamber was approximately 10^{-9} mbar, and the system was equipped with an Al/Mg standard twin anode material (Xr 3E2 twin Anode x-ray source). In this experiment, Mg Kα ($h\nu = 1253.6$ eV) was used as the radiation source, at a 50 eV pass energy; C 1s as an internal standard and Au 4f7/2 as an external standard were determined at 285.0 eV and 83.8 eV, respectively. Note that the samples were prepared by mounting and drying the sample solutions on an Si(111) wafer as a substrate.

2.5. Binding QD–IgG Ab molecule hybrid with target antigen

To assess the actual binding capacity of the IgG Ab-coated QD for identifying and labeling the model antigen microcystin-LR (volume z), the composite was reacted for 2 h with different molar ratios of an antigen (N_{Ag}), as follows.

$$N_{\mathrm{Ag}} = \frac{10\ \mu\mathrm{g}}{\mathrm{ml}} \times \frac{\mathrm{mol}}{995.2\ \mathrm{g}} \times \frac{6.023 \times 10^{23}\ \text{microcystin-LRs}}{\mathrm{mol}} \times (z)\ \mu\mathrm{l} \times \frac{\mathrm{g}}{10^{6}\ \mu\mathrm{g}} \times \frac{\mathrm{ml}}{10^{3}\ \mu\mathrm{l}}. \quad (4)$$

After completing the immunological recognition reaction, excess antigens were then separated from the entire complexes through size exclusion with a 100 kD cutoff membrane at 2000 rpm, and then analyzed using a hybrid ion trap-time of flight liquid chromatography mass spectrometer (LCMS-IT-TOF, Shimadzu). The operational method is further described in appendix B.

3. Results and discussion

3.1. Photoelectric behaviors of discrete QD nanocrystals and IgG Ab molecules

3.1.1. Optical behaviors of QD nanocrystals and IgG Ab molecules. Electron moves from the valence band (VB) to the conduction band (CB) by acquiring a sufficient photon energy that allows it to exceed the band gap; i.e., the difference in energy between the HOMO and LUMO, thereby creating positively charged holes in the valence band. When the excited electrons then relax to their ground state and electron–hole pairs (exciton) recombine by Coulomb interaction, energy is given off as a photon equal to the band gap energy, that is, photoluminescence occurs. The photoluminescence signal is thus a useful tool for monitoring the electron and hole transfer process [20].

EEM spectroscopic analysis was performed to explore the unique photoluminescence behavior as a fingerprint of the constituents for the IgG Ab molecule-encapsulated QD nanocrystal, and then to determine the most efficient photon energy for excitation and emission, as shown in figure 2. First, in order to eliminate the solvent effect on photoluminescence for the target fluorophore, the contour plot of the background EEM is depicted in figure 2(a). These water scattering peaks originate from Rayleigh scattering, in which the emission peaks occurred at the same wavelength as the excitation photon energy, and Raman scattering, in which a red shift to a longer wavelength is induced [21]. Both types of scattering

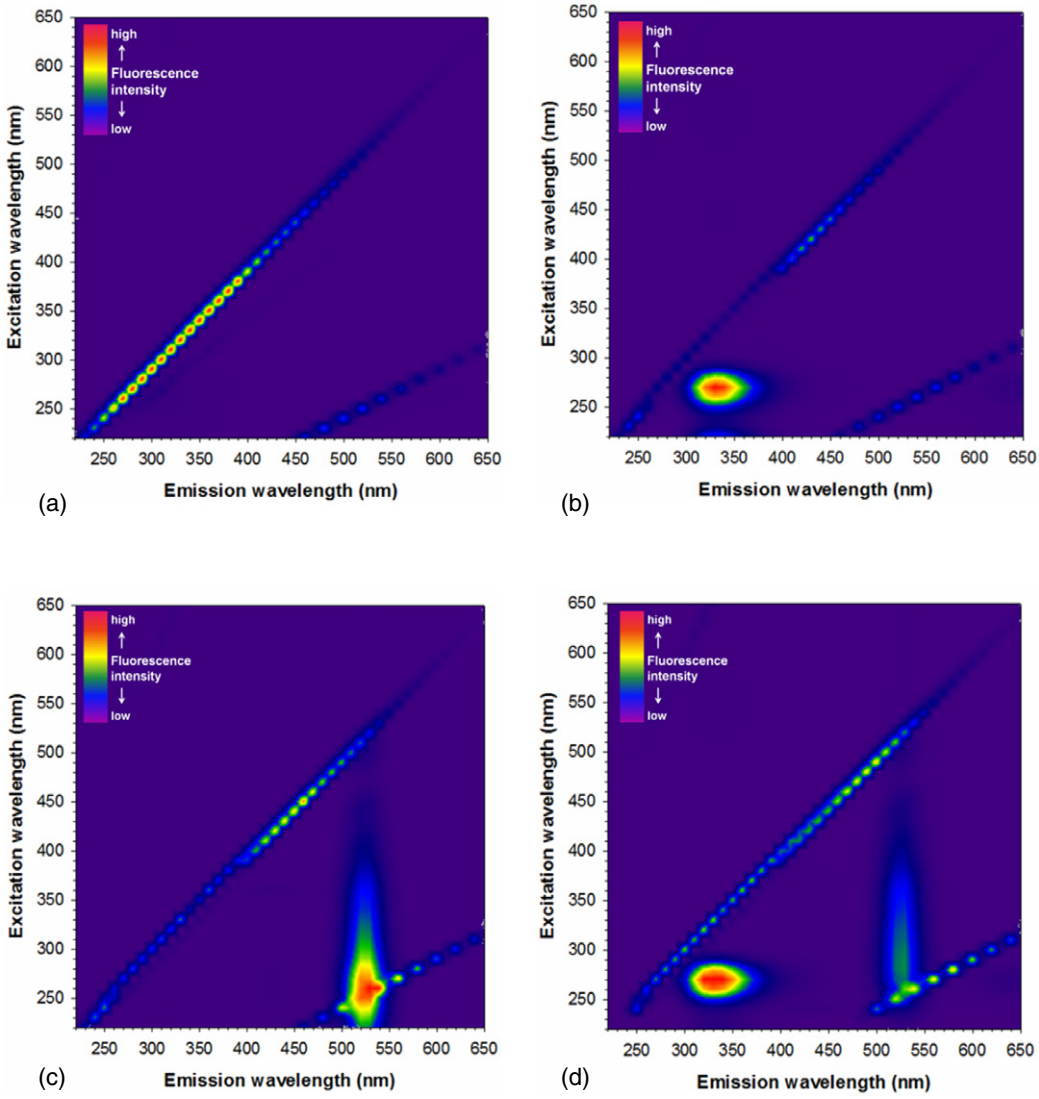

Figure 2. Contour plots of EEM for (a) 20 mM sodium tetraborate as solvent, (b) IgG Ab molecules, (c) QDs, and (d) IgG Ab molecule-encapsulated QDs. The 3D photoluminescence spectra were scanned at a scan speed of 1500 nm min^{-1}, with 5.0 nm excitation and emission slits, and 700 V PMT voltage.

are responsible for the optical interactions between the water molecules and the excited photon energy.

From the confined EEM area in the UV wavelength range of the IgG Ab molecule, via Stokes shift, the highest excitation band (λ_{ex}) was centered at 280 nm and the emission (λ_{em}) was recorded at 335 nm (figures 2(b) and E.1) in the given local aqueous environment. Note that the protein photoluminescence of IgG Ab molecules usually originates from two amino acids that contain aromatic side chains, such as tyrosine and tryptophan, which are natural fluorophores commonly found in almost all proteins [22]. Consequently, the emitted photoluminescence was found to be in proportion to the aromatic amino acid content and the total concentration of IgG Ab molecules (appendix C). On the other hand, figure 2(c) shows that QDs have broad excitation profiles, although a narrow emission wavelength range could be defined. The QDs utilized in this study (appendix D) were photoexcited at a wavelength of 400 nm in order to exclude the effects of water scattering and the emission of the photon energy by the IgG Ab molecules. With the defined excitation wavelength, the QD nanocrystals emitted green photoluminescence at 527 nm, originating from the CdSe core. Quantum confinement was accomplished by the ZnS shell, which has a large band gap that serves as a surface passivating layer and as a barrier that helps confine the electron and hole into the core [23]. The photoluminescence of the QDs was also shown to be proportionally responsive to its concentration (appendix C).

To estimate the optical band gap energy, the absorption and photoluminescence spectra are displayed in figure E.1. The band gap values deduced from the absorption onset and photoluminescence peak wavelengths are also summarized in table 1. Since the photoluminescence energy strongly depends on the fluorophore surface, in spite of having well defined quantum confinement [24], the band gap energies

Table 1. Optical and electrochemical parameters for evaluating band edge energies of IgG Ab molecules and QDs.

	Optical parameter				Electrochemical parameter		
	Absorption		Photoluminescence				
Compound	λ_{onset} (nm)[a]	Band gap (eV)[b]	λ_{peak} (nm)[c]	Band gap (eV)[b]	E^{ox}_{peak} (V)[d]	HOMO (eV)	LUMO (eV)
IgG Ab molecule	300	4.13	335	3.70	1.02	−5.40	−1.27
QD	467	2.66	527	2.35	1.42	−5.80	−3.14

[a] Onset value of absorption spectra in the range of visible to ultraviolet wavelengths.

[b] Band gap energies were obtained from the absorption onset or the photoluminescence peak value, calculated as $E_{band\ gap} = 1240/\text{wavelength}\lambda$ (nm).

[c] Photoluminescence on applying the excitation photon energy at 400 nm for QDs and 280 nm for IgG Ab molecules.

[d] Anodic peak potential as determined by means of cyclic voltammograms of a gold electrode (0.8 mm radius) in acetonitrile + 0.1 M $TBAPF_6$; potential sweep rate of 50 mV s^{-1} in the negative direction from the open circuit potential at room temperature.

obtained from the absorption onset values, 4.13 eV for IgG Ab molecules and 2.66 eV for QD nanocrystals, were utilized for this study.

3.1.2. Evaluation of band edge energies for QD nanocrystals and IgG Ab molecules. The optical parameters are closely related to electrochemistry [25, 26]. During the oxidation process, no anodic current will flow until the potential applied to accumulate charge reaches an onset value that corresponds to the HOMO of the VB edge; i.e., the ionization potential is an electrochemical parameter. On the other hand, the cathodic peak potential is correlated with the energy level of LUMO in the CB, which is filled with electrons as the applied potential is lowered (electron affinity). Here, figure E.2 shows that the absolute energetic band positions were determined via a series of electrochemical measurements. The HOMO energy levels from the vacuum level of the IgG Ab molecules and QDs were determined from the anodic peak potentials according to equation (1), and are summarized in table 1. It has been common practice to derive the LUMO value by subtracting the optical band from the HOMO level, due to the difficulty in determining the reduction potential [24]. Furthermore, in order to study the photoelectric response after attachment of IgG Ab molecules to the QD surface, the defined energy levels of each fluorophore are marked in the electronic band lineup of figure 5.

3.2. Verification of IgG Ab molecules docking on the QD nanocrystal surface

3.2.1. Conceptual configuration of IgG Ab molecule-tethered QD assembly as a building block. The conceptual configuration of the IgG Ab molecule-encapsulated QD hybrid as a fluorescent building block includes three compartments: the photoluminescence emitting center of the QD, an interfacial covalent linkage, and a biological recognition layer of IgG Ab molecules, as shown in figure 1.

IgG Ab molecules were reduced using DTT, which generates distinct fragments via the reduction of disulfide bonds to introduce free sulfhydryls. Two 75 kD partially cleaved chains were created from one Ab molecule, as a combination of a heavy chain (50 kD) and a light chain (25 kD) (inset of figure 1). The amino terminal of both the heavy and light chains in the functionalized IgG Ab still forms a variable region, which ensures a target antigen-binding site. The IgG Ab molecules irreversibly coupled with a QD via a heterobifunctional crosslinker are physically oriented outward from the QD surface, which constructs an immunological recognition layer to interact with two target ligands [14].

The number of functionalized IgG Ab molecules encapsulated on the QD surface as a bioactive layer is restricted due to steric accommodation [27], which should be further quantitatively analyzed to correctly interpret the biological recognition of the target antigen.

3.2.2. Verification of interface bridge between IgG Ab molecules and the QD nanocrystal surface. XPS was performed in order to validate the linkage of IgG Ab molecules with QDs (figure 1) by investigating the chemical composition of the surface [28]. Figure 3 displays the spectrum as a plot of the number of electrons versus the electron binding energy over a fixed range for (a) C 1s, (b) N 1s, (c) O 1s, (d) S 2p, (e) Zn 2p, and (f) Cd 3d.

Table F.1 summarizes the binding energies for the QDs, IgG Ab molecules, and QD/IgG Ab molecule conjugates observed at the atomic orbital in which the electron originates. Because each element has a unique binding energy, the chemical state can be determined based on the differences in the elemental binding energies, or chemical shifts, arising from variations in the chemical potential and polarizability of compounds in the surface. These binding energy shifts were previously investigated to adduce evidence for the formation of IgG Ab molecule-encapsulated QDs [29].

As seen in figure 3(b), overlap of the N 1s peak was observed in the lower binding range of Cd 3d due to the presence of unfiltered x-ray radiation [30]; therefore, the photoelectron lines of N 1s and Cd 3d cannot be used as indicators to estimate the bonding between QD nanocrystals and IgG Ab molecules.

The peak of the O 1s photoelectron line (figure 3(c)), however, shows a both shift and increase in its full width at half maximum (FWHM; QD = 3.7±0.1, QD/Ab complex = 4.2± 0.1). In the S 2p binding energy region depicted in figure 3(d), the photoelectron line of S 2p shifted toward a higher binding

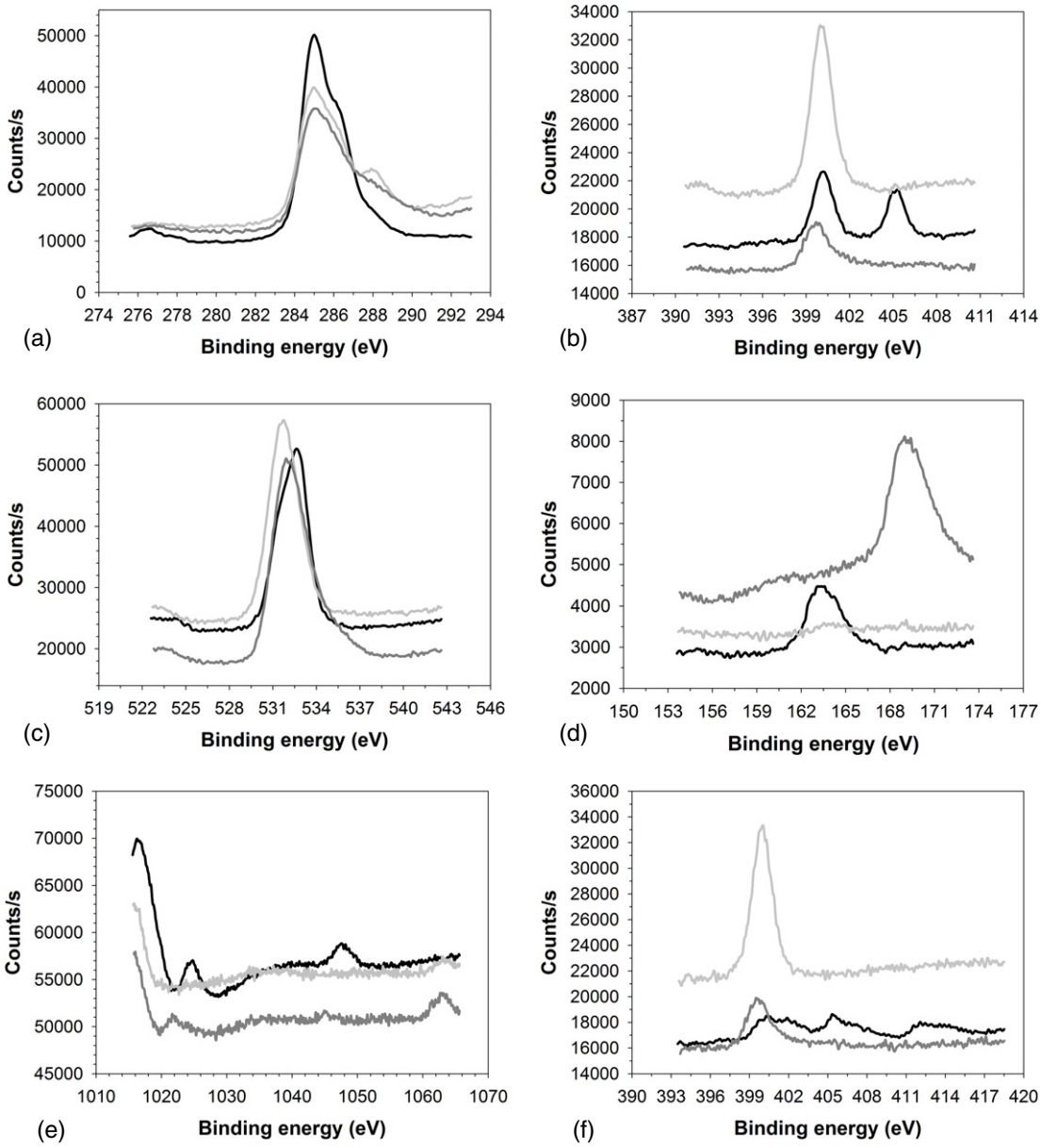

Figure 3. X-ray photoelectron spectrum of IgG Ab molecules (grey), QDs (black), and IgG Ab molecule-passivated QD hybrids (dark grey), illustrated in the fixed window for (a) C 1s, (b) N 1s, (c) O 1s, (d) S 2p, (e) Zn 2p, and (f) Cd 3d.

energy level after IgG Ab molecules were covalently reacted on the QD surface. The large shift strongly suggests that the atoms present in the QDs lost their valance charge and that the attractions in the electrons and nucleus increased, resulting from interactions with electronegatively charged Ab molecules. The shift of the S 2p binding energy peak and charge transfer is adequate evidence for proving the conjugation and formation of a QD/IgG Ab biocomplex. In addition, the presence and subtle shift of the major line of Zn arising from splitting the doublet spin orbit in the ionization of the p level at 1022 eV shows the possible bonding between QD and Ab, (figure 3(e)). Therefore, the spectral shift of O 1s, S 2p and Zn 2p may be evidence to verify the interaction and covalent binding between Ab and QD involving charge transfer.

3.3. Photoelectric interaction and response of IgG Ab molecule-encapsulated QD hybrid

Figure 4(a) illustrates the protein photoluminescence of the IgG Ab molecules bound to the surface of QDs under different molar ratios (N_{Ab}:N_{QD}) or for excess IgG Ab fragments that did not participate in the conjugation reaction. Whereas the intensity of emitted photons proportionally increased as IgG Ab molecules were encapsulated on the QD surface until a molar ratio for N_{Ab}:N_{QD} of six was attained, photoluminescence resulting from the excess fragments sharply rose compared to that of the composition ratio. This observation implies that the bioactive monolayer of IgG Ab molecules is inevitably coated on the QD surface due to limited steric accommodation; i.e., the most densely

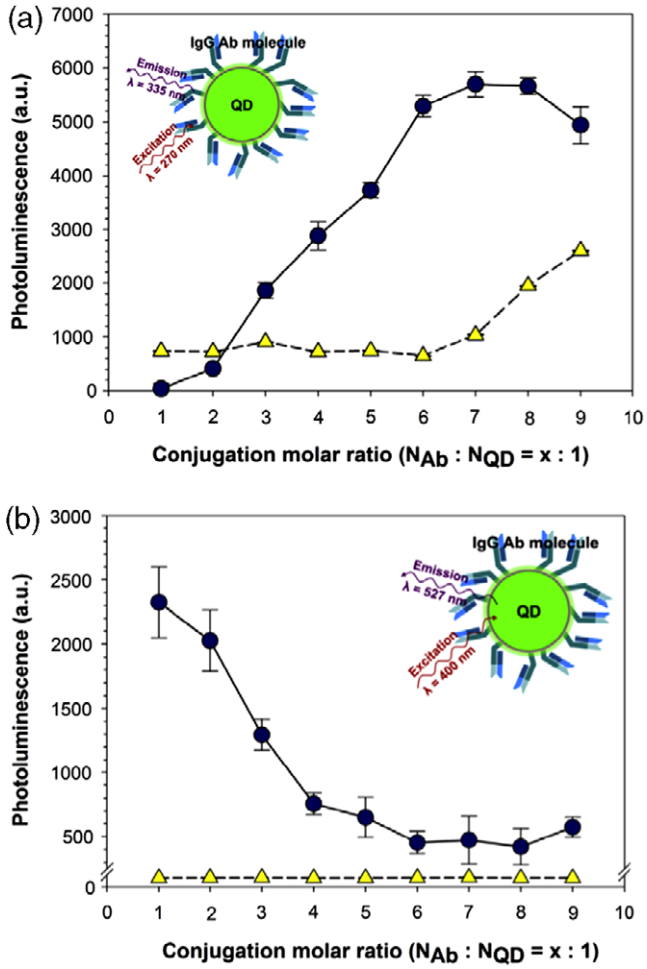

Figure 4. Spectroscopic responses of IgG Ab molecule-encapsulated QD assembly on introducing photon energy to the (a) biological recognition layer and (b) green photoluminescence emitting center. When the excess IgG Ab molecules were reacted on the QD surface with a stoichiometry-dependent conjugation, the (a) protein photoluminescence and (b) QD photoluminescence for the retentate (blue circle) including the entire conjugate, and the filtrate (yellow triangle) containing the unbound components through size exclusion were recorded.

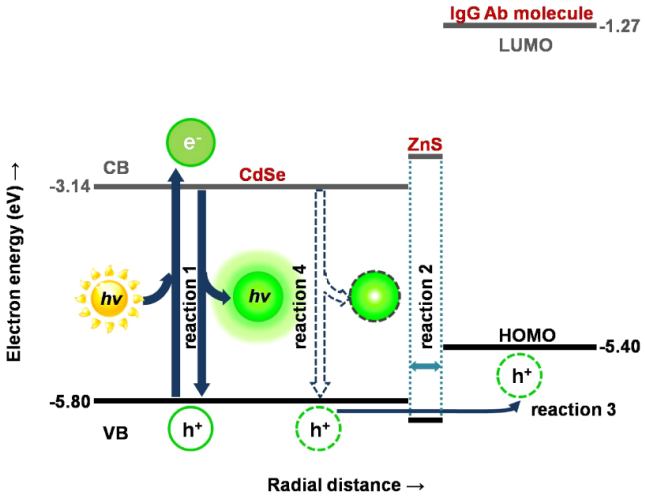

Figure 5. Energy diagram inside the IgG Ab molecule-encapsulated QD hybrid system. When the biomolecules are linked to the nanocrystal surface, the mechanism for generating the intrinsic QD photoluminescence (reaction 1: CdSe + $h\nu$ → CdSe ($h^+ + e^-$) → CdSe + $h\nu'$) changes, leading to a quenching event. This change originates from the photoinduced hole transfer from the VB of the CdSe core of QD to the HOMO of the IgG biomolecule (reaction 3: CdSe (h^+) + IgG Ab molecule → CdSe + IgG Ab molecule$^+$) due to construction of a new electronic trap, which accompanies the tunneling effect (reaction 2). The photogenerated hole transfer gives rise to a decrease of the emitting centers and nonradiative relaxation process (reaction 4), which thus brings about a decrease of QD photoluminescence.

packed biomolecular elements on the QD surface ensure the highest binding capacity for a target antigen by offering the most binding sites.

Interestingly, when a covalent interface bridge between the discrete QD nanocrystal and IgG Ab molecules was built, the intrinsic spectroscopic behavior of QDs underwent a significant change (figure 4(b)). The figure shows that the photoluminescence intensity of QDs considerably decreased as more IgG Ab molecules were attached to the QD. When the most densely packed IgG Ab molecules on the nanocrystal surface reached a molar ratio of six for N_{Ab}:N_{QD}, the number of photons emitted from the conjugated fluorophore decreased by 80%, compared to the spectral emission response of bare QDs. This observation is logical in that it corresponds to the number of IgG Ab molecules capped on the QD surface, as derived from monitoring the protein photoluminescence.

The decrease of photoluminescence of IgG Ab molecule-encapsulated QDs is closely related to electron and hole flow in response to the absorbed photons, which can be discussed in terms of the electronic level structure (figure 5). Since the HOMO and LUMO of IgG Ab molecules are energetically above the quantized state of the CdSe core of QDs, binding the biomolecules to the surface of a nanocrystal leads to the formation of a new surface electronic state (trap) [31–34]. From the energy level diagram, only holes can transfer from the VB of the nanocrystal to the HOMO of the IgG biomolecule, via the tunneling effect through a sufficiently thin ZnS shell and polymer coating [32, 34]. Conversely, it is evident that the photoexcited electrons are confined to the CB of the CdSe core due to the energy barrier created by the IgG Ab molecules, which is further supported by the fact that no spectral shift is observed when the photoluminescence of the QD was recorded as the amount of capped biomolecules increased. The photoinduced hole transfer reflects the decrease in the number of emitting centers in the CdSe core of nanocrystals, which consequently disrupts the exciton recombination process [34]. Furthermore, traps on the QD surface may bring about a nonradiative recombination process to create neutralization and stabilization through a Coulomb interaction [31–33]. Because the electronic structure of a capping ligand influences changes in the photoelectric behavior of a fluorescent nanocrystal due to induction of a new surface electronic state, the energy level of the capping molecule should thus be carefully considered and characterized. In

addition, the number of the molecules immobilized on the nanocrystal surface can then be derived by monitoring the photoluminescence of the fluorophore.

Although the most packed IgG Ab molecule-encapsulated QDs (6 N_{Ab}/N_{QD}) possess 12 target binding sites, only an 84.7% binding efficiency was observed in this study, as a result of the quantification of model antigens that reacted or not with the conjugate (data not shown). The unexpectedly low estimate is due to the steric hindrance and inaccessibility of target proteins to attach to available binding sites because of the randomly oriented immobilization of IgG Ab molecules on the nanocrystal surface through covalent conjugation [14].

4. Conclusions

In this study, an IgG Ab molecule-coated QD hybrid was characterized by monitoring the photoluminescence signal in order to provide a nondestructive analysis and thereby determine the most efficient configuration. Derivation of the optimum number of IgG Ab molecules to be packed onto the QD surface, representing the highest binding capacity, was found to contribute to a more cost-effective configuration, as opposed to existing conjugation processes that include matching excess biomolecules with a nanoparticle. During the formation of a biological recognition layer on the QD surface, the intrinsic photoluminescence of QD varied due to the altered photoelectric communication between the IgG Ab molecules and QDs, based on the rearranged electronic structure. Therefore, in applying the QD-based biomolecule hybrid, the energy level of the capping molecule should be carefully considered and characterized.

The critical significance of this study is that the profound photoelectric characterization approaches to both the bioactive region and photoluminescence emitting center in QD bioconjugates provide an effective tool for the manipulation and interpretation required for identifying and labeling a target protein. Furthermore, a more fundamental understanding of the electronic structure of the semiconductor/organic interface enables applications to be extended to numerous fields, including QD-based organic molecular electronics such as biosensors, displays, solar cells, and transistors.

Acknowledgments

This research was supported by a grant (07SeaHeroA01-01) from the Plant Technology Advancement Program funded by the Ministry of Land, Transport and Maritime Affairs.

Appendix A. Characterization of IgG Ab molecule-encapsulated QD assembly: gel electrophoresis

A gel electrophoresis was used to differentiate molecular entities based on their electrophoretic mobility, depending on physical characteristics such as size, mass, shape, and charge. To investigate the electrophoretic mobility of IgG biomolecule-passivated QDs, the gel electrophoresis was performed with QDs conjugated under different molar ratios of IgG Ab. The QDs used in this study had an estimated molecular weight of ∼1500–2000 kD; however, if it placed on a gel, the nanocrystals will migrate similarly to the 750 kD protein band. The molecular masses of the samples loaded on the gel are summarized in table A.1, in which the molecular weight (M.W.) of the QD is assumed to be 1500 kD. As shown in figure A.1, the image appeared smeared due to some diffusion effects. In addition, there were no significant differences in their electrophoretic mobilities, regardless of the

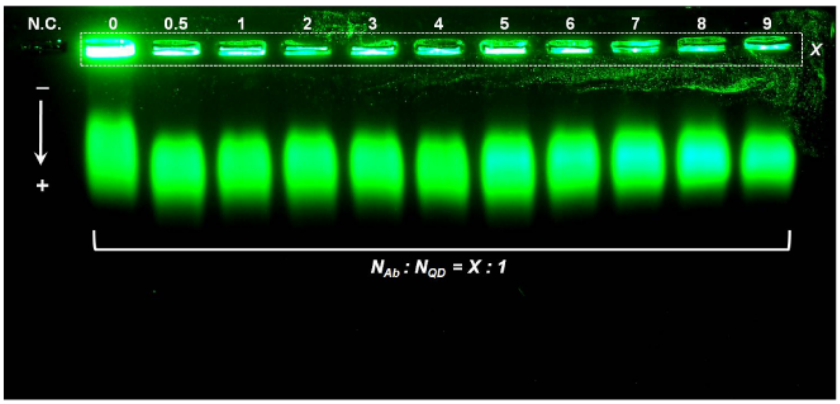

Figure A.1. Gel electrophoresis analysis of IgG molecule-encapsulated QDs, performed using a 10X loading dye on a 0.5% agarose gel at 100 V in a 0.5X TAE buffer.

Table A.1. Summarized molecular masses of IgG molecule-encapsulated QDs.

	N.C.	0	0.5	1	2	3	4	5	6	7	8	9
$M.W._{actual}$ (kD)	0	1500	1575	1650	1800	1950	2100	2250	2400	2550	2700	2850
$M.W._{gel}$ (kD)	0	750	825	900	1050	1200	1350	1500	1650	1800	1950	2100

supramolecular behavior. This impediment may be attributed to the high charge to mass ratio due to the strong charge characteristics of the nanocrystals [13].

Appendix B. Operation conditions for analysis of microcystin-LR as a target antigen using LCMS-IT-TOF

The mobile phase system consisted of HPLC grade water (solvent A) and HPLC grade acetonitrile (solvent B), both containing 0.1% formic acid (v/v). The gradient elution program started with 10% B and was maintained for 5 min, followed by a linear gradient increase from 10% B to 50% B over 15 min. The 50% B was then maintained for 10 min before returning to the initial mobile phase conditions of 10% B; the total run time was 30 min. Here, the injection volume was 10 μl and the flow rate was set at 0.15 ml min^{-1}. The separation of microcystin-LR was achieved using a chromatographic C18 column (Shimpack XR-ODS, Shimadzu) at a retention time of 15 min. The IT-TOF mass spectrometer was operated using an electrospray ionization (ESI) nanointerface in positive mode as follows: probe voltage of +4.5 kV, curved desolvation line (CDL) and the block heater temperatures of 200 °C, CDL voltage of +25 V, drying gas pressure of 200 kPa, and nebulizing gas flow of 1.5 l min^{-1}. A quadrupole MS spectrum (MS^1) was acquired for precursor molecular ions having m/z = 498.2, which are the doubly charged ions characterized for microcystin-LR.

Appendix C. Quantitative analysis of intrinsic photoluminescence of individual components: IgG Ab molecules and QDs

A quantitative analysis of the discrete components of IgG biomolecules and QDs was performed to verify that the photoluminescence intensities of both fluorophores were proportionally responsive to their concentration, as shown in figure C.1. To ensure the reliability of this assessment, the limit of detection (LOD) and limit of quantitation (LOQ) need to be established, based on standards established by the International Union of Pure and Applied Chemistry (IUPAC) and the American Chemical Society (ACS) [35]. As a result, the protein photoluminescence ($\lambda_{ex}/\lambda_{em}$ = 280/335 nm) was deemed suitable for determining the concentration of IgG Ab molecules, with a high sensitivity (403.54 photoluminescence intensity per μg ml^{-1} of IgG Ab). In addition, the lower LOD and LOQ were determined to be 0.76 μg ml^{-1} and 1.14 μg ml^{-1}, respectively (99.865% confidence level, k_{LOD} = 3 and k_{LOQ} = 10). On the other hand, the QDs also sensitively reacted with the photon energy ($\lambda_{ex}/\lambda_{em}$ = 400/527 nm) at 376.63 photoluminescence intensity per nM of QD with 0.010 nM LOD and 0.012 nM LOQ.

Appendix D. Characterization of QDs and IgG Ab-encapsulated QD hybrids: TEM

The surface of the CdSe/ZnS QDs used in this study (Qdot525 Antibody Conjugation Kit, Invitrogen) was encapsulated with ligands such as TOPO (length = 0.7 nm)/TOP, AMP, and functional groups of methoxyl 70% and NH_2 30% (figure 1), which allow the nanocrystals to be water-soluble and to conjugate with biomolecules. The QD nanocrystals of the colloidal suspensions show a lattice structure 5 nm in size, which indicates the size of only the inorganic components, CdSe core, and ZnS shell, as shown in figure D.1. Although the IgG Ab molecule-encapsulated QD assembly was also visualized by TEM (data not shown), the characterization was ultimately unsuccessful due to the dryness of the biological active layer [13].

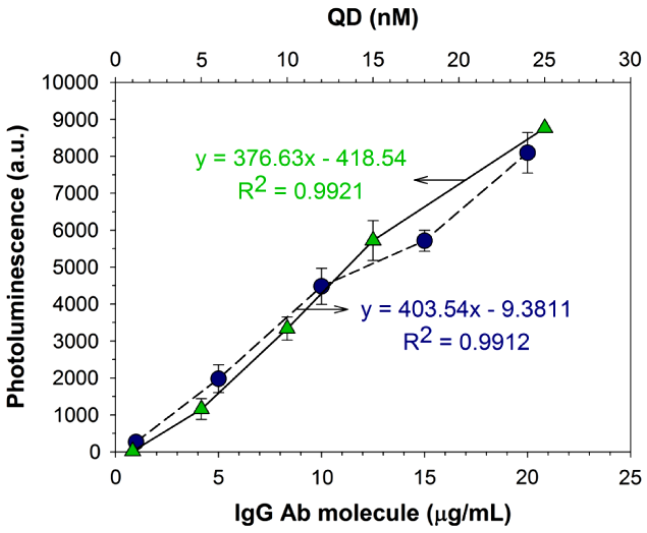

Figure C.1. Photoluminescence response to concentration of IgG Ab molecules (blue circles) and QD (green triangles).

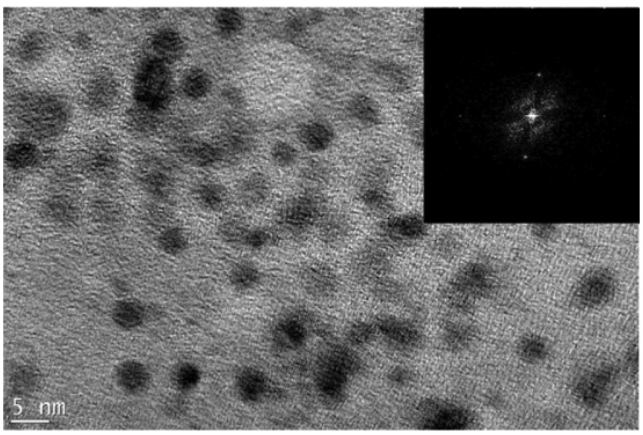

Figure D.1. TEM image of QD nanocrystal. TEM analysis of the sample dispersed on a carbon-coated CU TEM grid was performed using a JEM-2100 (Joel) with an LaB6 filament at a 200 kV acceleration voltage.

Appendix E. Determination of band edge energies for QD nanocrystals and IgG Ab molecules

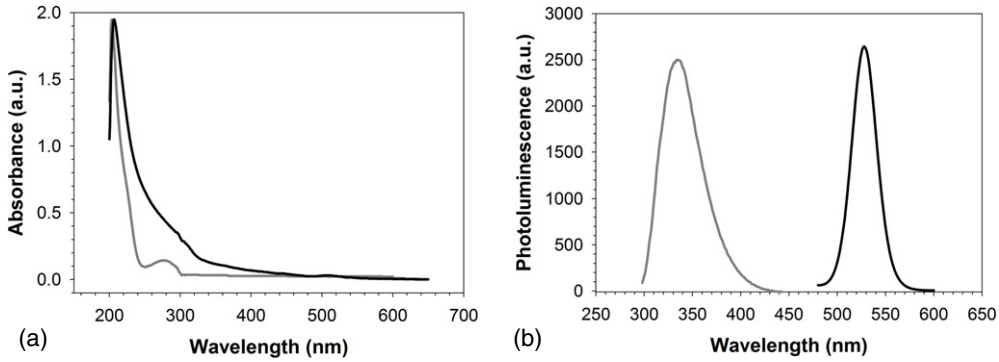

Figure E.1. Optical behavior of IgG Ab molecules (dark grey) and QD nanocrystals (black), using (A) absorption spectra in the visible to ultraviolet range and (B) photoluminescence by applying an excitation photon energy at 400 nm for QDs and 280 nm for IgG Ab molecules. Band gap energies were obtained from the absorption onset values and the photoluminescence peak value, calculated as $E_{\text{band gap}} = h\upsilon = hc/\lambda = 1240/\lambda$.

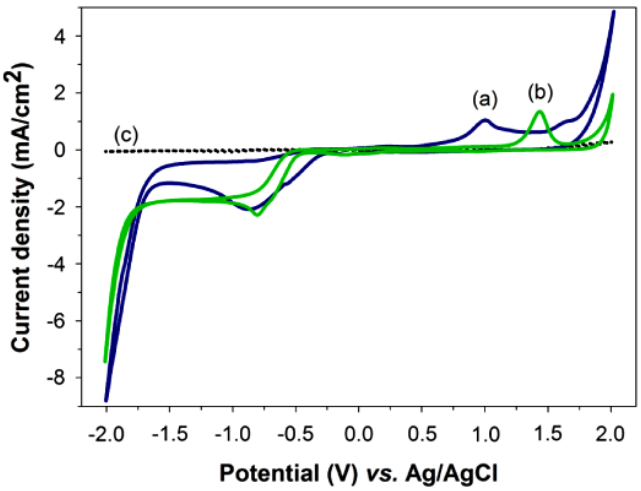

Figure E.2. Cyclic voltammograms of a gold electrode (0.8 mm radius) in acetonitrile + 0.1 M $TBAPF_6$ containing (a) IgG Ab molecules, (b) monodispersed QDs, and (c) a blank electrolyte. The potential sweep rate was 50 mV s^{-1} in the negative direction from the open circuit potential at room temperature.

Appendix F. Verification of covalent binding between IgG Ab molecules and QD nanocrystal surface

References

[1] Bruchez M Jr, Moronne M, Gin P, Weiss S and Alivisatos A P 1998 Semiconductor nanocrystals as fluorescent biological labels *Science* **281** 2013–6

[2] Dabbousi B O, Rodriguez-Viejo J, Mikulec F V, Heine J R, Mattoussi H, Ober R, Jensen K F and Bawendi M G 1997 (CdSe)ZnS core–shell quantum dots: synthesis and characterization of a size series of highly luminescent nanocrystallites *J. Phys. Chem.* B **101** 9463–75

[3] Leatherdale C A, Woo W K, Mikulec F V and Bawendi M G 2002 On the absorption cross section of CdSe nanocrystal quantum dots *J. Phys. Chem.* B **106** 7619–22

[4] Cai W and Chen X 2008 Preparation of peptide-conjugated quantum dots for tumor vasculature-targeted imaging *Nat. Protoc.* **3** 89–96

[5] Michalet X, Pinaud F F, Bentolila L A, Tsay J M, Doose S, Li J J, Sundaresan G, Wu A M, Gambhir S S and Weiss S 2005 Quantum dots for live cells, *in vivo* imaging, and diagnostics *Science* **307** 538–44

[6] So M K, Xu C, Loening A M, Gambhir S S and Rao J 2006 Self-illuminating quantum dot conjugates for *in vivo* imaging *Nat. Biotechnol.* **24** 339–43

[7] Park J-S, Cho M K, Lee E J, Ahn K-Y, Lee K E, Jung J H, Cho Y, Han S-S, Kim Y K and Lee J 2009 A highly sensitive and selective diagnostic assay based on virus nanoparticles *Nat. Nanotechnol.* **4** 259–64

[8] Yu H W, Lee J, Kim S, Nguyen G H and Kim I S 2009 Electrochemical immunoassay using quantum dot/antibody probe for identification of cyanobacterial hepatotoxin microcystin-LR *Anal. Bioanal. Chem.* **394** 2173–81

[9] Zhang C-Y and Johnson L W 2009 Single quantum-dot-based aptameric nanosensor for cocaine *Anal. Chem.* **81** 3051–5

[10] Caruge J M, Halpert J E, Wood V, Bulovic V and Bawendi M G 2008 Colloidal quantum-dot light-emitting diodes with metal-oxide charge transport layers *Nat. Photon.* **2** 247–50

[11] Sun Q, Wang Y A, Li L S, Wang D, Zhu T, Xu J, Yang C and Li Y 2007 Bright, multicoloured light-emitting diodes based on quantum dots *Nat. Photon.* **1** 717–22

[12] Gratzel M 2001 Photoelectrochemical cells *Nature* **414** 338–44

Table F.1. Summarized binding energies of QDs, IgG Ab molecules, and IgG Ab molecule-encapsulated QD complexes from XPS measurements.

	Binding energy (eV)							
Compound	C 1s	N 1s	O 1s	S 2p	Zn $2p_{3/2}$	Zn $2p_{1/2}$	Cd $3d_{5/2}$	Cd $3d_{3/2}$
QD	285.1 ± 0.1	399.5 ± 0.5	405.1 ± 0.2	531.9 ± 0.2	161.6 ± 0.4	1021.9 ± 0.5	1045.1 ± 0.5	405.0 ± 0.6	411.5 ± 0.6
IgG Ab molecule	285.0 ± 0.0	399.7 ± 0.4	—	531.5 ± 0.3	—	—	—	—	—
QD/IgG Ab assembly	285.0 ± 0.0	399.0 ± 0.3	—	531.3 ± 0.5	168.6 ± 0.5	1021.7 ± 0.4	—	399.1 ± 0.6	—

[13] Calabretta M, Jamison J A, Falkner J C, Liu Y, Yuhas B D, Matthews K S and Colvin V L 2005 Analytical ultracentrifugation for characterizing nanocrystals and their bioconjugates *Nano Lett.* **5** 963–7
[14] Pathak S, Davidson M C and Silva G A 2007 Characterization of the functional binding properties of antibody conjugated quantum dots *Nano Lett.* **7** 1839–45
[15] Wang S, Mamedova N, Kotov N A, Chen W and Studer J 2002 Antigen/antibody immunocomplex from CdTe nanoparticle bioconjugates *Nano Lett.* **2** 817–22
[16] Wu H, Liu G, Wang J and Lin Y 2007 Quantum-dots based electrochemical immunoassay of interleukin-1α *Electrochem. Commun.* **9** 1573–7
[17] Pommerehne J N, Horst V, Werner G, Rainer F M, Heinz B S, Michael P and Daub J G 1995 Efficient two layer LEDs on a polymer blend basis *Adv. Mater.* **7** 551–4
[18] Bredas J L, Silbey R, Boudreaux D S and Chance R R 1983 Chain-length dependence of electronic and electrochemical properties of conjugated systems: polyacetylene, polyphenylene, polythiophene, and polypyrrole *J. Am. Chem. Soc.* **105** 6555–9
[19] Gritzner G and Kuta J 1984 Recommendations on reporting electrode potentials in nonaqueous solvents *Pure Appl. Chem.* **56** 461–6
[20] Joseph R L 2006 *Principles of Fluorescence Spectroscopy* (Berlin: Springer)
[21] Zepp R G, Sheldon W M and Moran M A 2004 Dissolved organic fluorophores in southeastern US coastal waters: correction method for eliminating Rayleigh and Raman scattering peaks in excitation-emission matrices *Mar. Chem.* **89** 15–36
[22] Mann T L and Krull U J 2003 Fluorescence polarization spectroscopy in protein analysis *Analyst* **128** 313–7
[23] Korsunska N E, Dybiec M, Zhukov L, Ostapenko S and Zhukov T 2005 Reversible and non-reversible photo-enhanced luminescence in CdSe/ZnS quantum dots *Semicond. Sci. Technol.* **20** 876–81
[24] Kucur E, Riegler J, Urban G A and Nann T 2003 Determination of quantum confinement in CdSe nanocrystals by cyclic voltammetry *J. Chem. Phys.* **119** 2333–7
[25] Bae Y, Myung N and Bard A J 2004 Electrochemistry and electrogenerated chemiluminescence of CdTe nanoparticles *Nano Lett.* **4** 1153–61
[26] Eckhardt H, Shacklette L W, Jen K Y and Elsenbaumer R L 1989 The electronic and electrochemical properties of poly(phenylene vinylenes) and poly(thienylene vinylenes): an experimental and theoretical study *J. Chem. Phys.* **91** 1303–15
[27] Swain M D, Octain J and Benson D E 2008 Unimolecular, soluble semiconductor nanoparticle-based biosensors for thrombin using charge/electron transfer *Bioconjug. Chem.* **19** 2520–6
[28] Kulkarni S K, Ethiraj A S, Kharrazi S, Deobagkar D N and Deobagkar D D 2005 Synthesis and spectral properties of DNA capped CdS nanoparticles in aqueous and non-aqueous media *Biosens. Bioelectron.* **21** 95–102
[29] Moulder J F, Stickle W F, Sobol P E and Bomben K D 1995 *Handbook of X-ray Photoelectron Spectroscopy* (Chanhassen, MN: Physical Electronics)
[30] Wagner C D, Riggs W M, Davis L E, Moulder J F and Mullenberg G E 1978 *Handbook of X-ray Photoelectron Spectroscopy* (Waltham, MA: Perkin-Elmer Corporation)
[31] Poznyak S K, Osipovich N P, Shavel A, Talapin D V, Gao M, Eychmuller A and Gaponik N 2005 Size-dependent electrochemical behavior of thiol-capped CdTe nanocrystals in aqueous solution *J. Chem. Phys.* B **109** 1094–100
[32] Schmelz O, Mews A, Basche T, Herrmann A and Mullen K 2001 Supramolecular complexes from CdSe nanocrystals and organic fluorophors *Langmuir* **17** 2861–5
[33] Zen'kevich E I, Sagun E I, Yarovoi A A, Shul'ga A M, Knyukshto V N, Stupak A P and von Borczyskowski C 2007 Photoinduced relaxation processes in complexes based on semiconductor CdSe nanocrystals and organic molecules *Opt. Spectrosc.* **103** 958–68
[34] Zhang Y, Jing P, Zeng Q, Sun Y, Su H, Wang Y A, Kong X, Zhao J and Zhang H 2009 Photoluminescence quenching of CdSe core/shell quantum dots by hole transporting materials *J. Chem. Phys.* C **113** 1886–90
[35] Mocak J, Bond A M, Mitchell S and Scollary G 1997 A statistical overview of standard (IUPAC and ACS) and new procedures for determining the limits of detection and quantification: application to voltammetric and stripping techniques *Pure Appl. Chem.* **69** 292–328
[36] Bonasio R, Carman C V, Kim E, Sage P T, Love K R, Mempel T R, Springer T A and von Andrian U H 2007 Specific and covalent labeling of a membrane protein with organic fluorochromes and quantum dots *Proc. Natl Acad. Sci.* **104** 14753–8
[37] Rhyner M N, Smith A M, Gao X, Mao H, Yang L and Nie S 2006 Quantum dots and multifunctional nanoparticles: new contrast agents for tumor imaging *Nanomedicine* **1** 209–17